Polarized and unpolarized neutron-scattering study of the dynamical spin susceptibility of $YBa_2Cu_3O_7$

H. F. Fong
Department of Physics, Princeton University, Princeton, New Jersey 08544

B. Keimer
Department of Physics, Princeton University, Princeton, New Jersey 08544
and Department of Physics, Brookhaven National Laboratory, Upton, New York 11973

D. Reznik
Department of Physics, Brookhaven National Laboratory, Upton, New York 11973
and National Institute of Standards and Technology, Gaithersburg, Maryland 20899

D. L. Milius and I. A. Aksay
Department of Chemical Engineering, Princeton University, Princeton, New Jersey 08544
(Received 4 January 1996)

We report an extensive study of magnetic excitations in fully oxygenated $YBa_2Cu_3O_7$, using neutron scattering with and without spin polarization analysis. By calibrating the measured magnetic intensity against calculated structure factors of optical phonons and against antiferromagnetic spin waves measured in the same crystal after deoxygenation to $YBa_2Cu_3O_{6.2}$, we establish an absolute intensity scale for the dynamical spin susceptibility, $\chi''(\mathbf{q},\omega)$. The integrated spectral weight of the sharp magnetic resonance at $\hbar\omega=40$ meV and $\mathbf{q}_\parallel=(\pi/a,\pi/a)$ in the superconducting state is $\int d(\hbar\omega)\chi''_{\rm res}(\mathbf{q},\omega)=(0.52\pm0.1)$ at low temperatures. The energy and spectral weight of the resonance are measured up to $T=0.8T_c$. The resonance disappears in the normal state, and a conservative upper limit of 30 states/eV is established for the normal state dynamical susceptibility at $\mathbf{q}_\parallel=(\pi/a,\pi/a)$ and 10 meV$\leq\hbar\omega\leq$40 meV. Our results are compared to previous neutron-scattering data on $YBa_2Cu_3O_7$, theoretical interpretations of NMR data and current models of the 40 meV resonance. [S0163-1829(96)03133-5]

I. INTRODUCTION

The importance of electron-electron interactions in the cuprate superconductors is now generally recognized. Due to strong electronic correlations the conventional (one-electron) theory of metals must be partially or completely revised to yield a description of these materials. A direct experimental manifestation of electron-electron interactions is an energy- and momentum-dependent enhancement of the dynamical spin susceptibility whose imaginary part, $\chi''(\mathbf{q},\omega)$, is measured by neutron scattering as a function of momentum $\mathbf{q}$ and energy $\hbar\omega$.

Neutron-scattering experiments at the Brookhaven[1–3] and Grenoble[4] reactors over the past several years have resulted in a detailed picture of the evolution of $\chi''(\mathbf{q},\omega)$ with carrier density in the underdoped $YBa_2Cu_3O_{6+\delta}$ system. Studies of the optimally doped compound ($\delta\sim1$) have proven to be difficult. Rossat-Mignod and collaborators[5] were the first to investigate this compound and reported a broad, weakly temperature-dependent peak around $\hbar\omega=30$ meV and $\mathbf{q}_{\parallel0}=(1/2,1/2)$ in the normal state. [Throughout this article we quote the momentum transfer indices (H,K,L) in reciprocal-lattice units (r.l.u.), that is, in units of the reciprocal-lattice vectors $a^*=2\pi/a\sim2\pi/b=1.63$ Å^{-1} and $c^*=2\pi/c=0.54$ Å^{-1}. $\mathbf{q}_{\parallel0}$ thus corresponds to the momentum transfer $(\pi/a,\pi/a)$ parallel to the CuO_2 layers.] In addition, they discovered a sharp enhancement of $\chi''(\mathbf{q}_{\parallel0},\omega)$ in the superconducting state at an energy around 40 meV. Different normal-state spectra were reported by Sato *et al.*[6] and Mook *et al.*[7,8] Instead of the broad 30 meV normal-state peak the latter authors reported energy-independent ''continua'' in both the normal and the superconducting states. Mook *et al.*[7] also investigated the temperature dependence of the 40 meV magnetic excitation, confirmed its magnetic origin by polarization analysis and claimed that it remains sharp in energy and centered around 40 meV in the normal state. More recently published data[8] still showed a sharp spin-flip signal at 41 meV in the normal state, though its origin appeared to be less clear. We[9,10] recently developed a new geometry for magnetic scattering experiments in $YBa_2Cu_3O_7$ and showed that, contrary to the claim of Mook *et al.*, the 40 meV resonance disappears in the normal state, which implies that the resonance is a novel signature of the superconducting state. Similar conclusions were reached by Bourges *et al.*[11] This observation has made a detailed theoretical interpretation of the resonance possible, and several models have been proposed in response to our work. These models fall into three categories.

The first model attributes the magnetic resonance to the creation of a quasiparticle-quasihole pair which leads to a neutron energy loss of $|\mathbf{\Delta_k}|+|\mathbf{\Delta_{k+q}}|$, where $\mathbf{\Delta_k}$ is the momentum-dependent superconducting energy gap and $\mathbf{q}$ separates the points on the Fermi surface where the quasiparticles are created.[9,12–16] If this interpretation is correct, the

neutron experiment actually measures both the magnitude and the phase of the superconducting energy gap. The coherence factor for this process necessitates a sign reversal of the energy gap function on the Fermi surface; without a sign reversal the cross section for this process is strongly suppressed. It was pointed out[13] that pair production generally only produces a step in χ'' as a function of ω. Additional circumstances such as final-state interactions between the quasiparticles[12–14] or nesting effects[15] must be invoked in order to explain the observed sharp peak in χ''. In the former case the magnetic resonance can be thought of as arising from a quasiparticle-quasihole bound state (triplet exciton).

In the second model the resonance is due to a collective mode whose existence follows from special symmetry properties of the Hubbard model.[17] The mode couples to the neutron through a particle-particle channel which is closed in the normal state, but opens in the superconducting state. In the framework of this model, observation of this mode by magnetic neutron scattering also implies d-wave symmetry of the gap function.

In the third model $YBa_2Cu_3O_7$ is close to an antiferromagnetic instability, and the magnetic excitation can be thought of as a spin wave.[18] The spin wave is overdamped in the normal state, but sharpens in the superconducting state as the energy gap removes particle-hole decay channels. In this picture 40 meV is the ''spin-gap'' energy.

In this work we give a detailed account of our experiments and present new unpolarized and polarized beam experiments which further constrain theoretical interpretations of the 40 meV resonance. Previously reported normal-state features in the neutron-scattering cross section, i.e., the broad 30 meV peak of Ref. 5 and the sharp 41 meV peak in the normal state of Refs. 7 and 8 are explicitly identified as arising from phonon scattering and accidental Bragg scattering, respectively. By careful normalization to phonon structure factors and antiferromagnetic spin waves (measured in the same crystal after deoxygenation) we further establish an absolute scale for the dynamical susceptibility and determine the spectral weight of the 40 meV resonance.

The work is organized as follows. After describing the characterization of our samples in Sec. II and details of the experiments (especially the polarized beam experiments) in Sec. III, we discuss the two different methods we use to calibrate the absolute intensity scale (Sec. IV). In Sec. V we first present a thorough discussion of the background in both polarized and unpolarized neutron-scattering experiments on $YBa_2Cu_3O_7$. Section V further contains polarized and unpolarized beam measurements of the temperature dependence of the resonance energy and absolute spectral weight, as well as quantitative limits on the normal-state dynamical susceptibility. In Sec. VI our results are compared to current interpretations of NMR data and discussed in the light of the above-mentioned models.

II. SAMPLE CHARACTERIZATION

Our samples were two single crystals of volumes $\sim$2.5 and $\sim$10 cm^3, respectively. The synthesis and processing of these crystals as well as studies of their microstructures and elemental compositions are described elsewhere.[19] Both crystals have mosaic spreads of $\sim$2° (full width at half maximum). The large crystal also has some smaller domains as far as 5° away from the main domain. The uniform susceptibility of a smaller crystal prepared under identical conditions is shown in Fig. 1. (The crystals used in the neutron experiments are too large to fit into a magnetometer.) The superconducting transition temperature is 93.0 K, and the transition width is $\sim$0.25 K, indicating excellent superconducting properties.

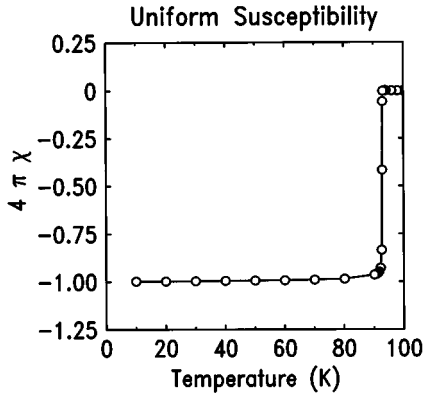

FIG. 1. Uniform susceptibility of a small $YBa_2Cu_3O_7$ crystal prepared under identical conditions as the specimens used in our neutron experiments, measured by SQUID magnetometry on field cooling.

An estimate of the oxygen content (δ in $YBa_2Cu_3O_{6+\delta}$) of our crystals can be obtained by comparing the measured T_c=93.0 K and room-temperature c-axis lattice constant (11.679 Å) to various calibrations reported in the literature. Since these calibrations differ somewhat, such a comparison carries an error of $\sim$0.05 for δ. The initial calibration by Cava *et al.*[20] quotes c=11.70 Å for $\delta\sim$1. Later Jorgensen *et al.*[21] obtained c=11.680 Å for δ=0.93. Finally Altendorf *et al.*[23] find c=11.689 Å for a crystal with δ=0.99 and T_c=92.8 K, a transition temperature very similar to the one we find in our samples. On balance, these comparisons indicate that $\delta\gtrsim$0.95 in our crystal.

A very powerful indicator of both sample quality and oxygenation is the superconductivity-induced softening of certain phonons, as extensive Raman scattering studies have shown that these effects are extremely sensitive to both the oxygen content and the presence of impurities. The softening of the 42.5 meV oxygen vibration below T_c has been particularly well characterized.[22–25] In Fig. 2(a) of Ref. 25 we have compared the Raman data of Altendorf *et al.*[23] taken on the above-mentioned high-quality $YBa_2Cu_3O_{6.99}$ crystal to neutron data taken on our sample and found excellent agreement. We have also quantitatively reproduced[25] the phonon softening measurements of Ref. 24 on a sample which is labeled $YBa_2Cu_3O_7$ over an extended range of **q**, whereas data taken on a $YBa_2Cu_3O_{6.92}$ sample strikingly disagree with ours. These observations again indicate that $\delta\sim$1 in our crystal. We further conclude that our large samples are as homogeneous and free of impurities as the best samples thus far studied by Raman scattering.

After the experiments in the fully oxygenated state were completed, the large sample was kept at temperatures between 675 and 750 °C under Ar flow for 10 days. After this heat treatment the oxygen content was δ=0.2 according to

the c-axis lattice constant (11.821 Å). High-resolution neutron diffraction further revealed that the crystal was tetragonal. The Néel temperature of the deoxygenated sample was 390 K, as expected in this range of oxygen concentration.[1,2]

III. EXPERIMENTAL DETAILS

The experiments were carried out at the High Flux Beam Reactor at the Brookhaven National Laboratory on the H4M, H7, and H8 spectrometers. The beam collimations were 40′-40′-80′-80′ throughout. In the unpolarized beam experiments the beam was monochromated and analyzed by pyrolytic graphite crystals, and the final energy was fixed at 30.5 meV. A pyrolytic graphite filter was placed behind the sample in order to eliminate higher-order contamination of the scattered beam.

In the polarized beam experiments[26] the neutron beam was polarized by a Heusler crystal, which Bragg diffracts only neutrons of a specific (vertical) spin-polarization direction. Before impinging on the sample the beam polarization is maintained [vertical field (VF)] or rotated by 90° [horizontal field (HF)] by guide fields. After scattering from the sample the beam polarization is again maintained or rotated back by 90°, respectively. The beam then traverses a flipper (a set of coils capable of flipping the neutron spin polarization by 180°), and the final beam polarization is analyzed by a Heusler crystal which Bragg reflects only neutrons whose polarization direction is the same as that of the original beam (after the monochromator). In order to optimize the beam polarization the final energy was kept fixed at 28 meV.

Because of limitations of the apparatus the beam polarization is always incomplete and is usually parametrized as (FR -1)/(FR$+1$), where FR is the ''flipping ratio.'' When the flipper is on, the spin-flip (SF) cross section is measured, superposed by a polarization ''leakage'' contribution from non-spin-flip (NSF) scattering events (single and multiple phonon scattering), a contribution from nuclear spin incoherent scattering (NSI), and an extrinsic background (B). B itself has several different origins: ''fast'' neutrons which reach the detector without scattering from the sample, neutrons that scatter elastically from the sample and incoherently from monochromator or analyzer, etc. Because of polarization terms in the coherent magnetic scattering cross section only half of the magnetic contribution (M) is measured for vertical guide field, whereas for HF the full contribution is measured. When the flipper is on and the flipping ratio is not too small, one obtains[26]

$$I_{\mathrm{HF}}=M+\frac{2}{3}\,\mathrm{NSI}+\frac{\mathrm{NSF}}{\mathrm{FR}}+B,$$

$$I_{\mathrm{VF}}=\frac{1}{2}\,M+\frac{2}{3}\,\mathrm{NSI}+\frac{\mathrm{NSF}}{\mathrm{FR}}+B. \qquad (1)$$

The standard method of extracting the magnetic contribution to the cross section is to subtract I_{VF} from I_{HF}, which yields $M/2$. The disadvantage of giving up a factor of 2 in intensity is more than compensated by the advantage of not having to attempt to determine the other three contributions to I_{HF} separately. The latter (nonstandard) method was chosen by Mook *et al.*[7] and yields better counting statistics at the expense of systematic errors (especially in measuring B). This will be discussed in Sec. V A.

Even if the standard HF-VF method is used a small correction must be applied, as the flipping ratios for HF and VF are not precisely identical: The HF flipping ratio is ~5% lower because of fringing effects in the guide fields. Our data were taken in several separate runs with VF FR's in the range 31–35 (corresponding to ~95% beam polarization). This should be compared to a FR of 11 (~80% beam polarization) in the work of Mook *et al.* In the superconducting state additional care must be taken to avoid beam depolarization when flux trapped in the sample is offset with respect to the guide field in the course of a scan. In our experiments the samples were field cooled and turned by less than 10° during a scan. By checking the FR at several nuclear Bragg reflections in the superconducting state we verified that under these conditions beam depolarization by trapped flux is negligible.

IV. ABSOLUTE INTENSITY SCALE

A. Phonon structure factors

Since the cross sections for both nuclear and magnetic neutron scattering are very well understood, the observed intensity of magnetically scattered neutrons, which partially depends on geometrical factors such as the sample size, can be normalized to the intensity of neutrons which undergo nuclear scattering events. In magnetic diffraction, normalization to nuclear Bragg reflections is standard practice for the determination of ordered moments. Similarly, a normalization to phonon intensities can be used to extract the absolute magnetic susceptibility from inelastic magnetic neutron-scattering data. In $La_{1.85}Sr_{0.15}CuO_4$ magnetic excitations of very low energy are observed, and normalization to acoustic phonons has been used to establish an absolute intensity scale.[27] For $YBa_2Cu_3O_7$, where such low-energy magnetic excitations have not yet been conclusively observed by neutron scattering, this procedure would be unreliable due to large energy and momentum-dependent resolution corrections.

Fortunately, Fong *et al.*[9] found that the 40 meV magnetic resonance is very close in energy to a nondispersive optical phonon mode at 42.5 meV whose eigenvector is relatively simple. Moreover, the phonon cross section peaks at almost the same point in reciprocal space as the magnetic resonance. Corrections for resolution effects are thus small, and the 42.5 meV phonon can serve as a good ''standard candle'' for the cross section of the resonance.

With the dual goal of normalizing the magnetic intensity and achieving a reliable background subtraction for unpolarized beam experiments we have carried out detailed lattice dynamical calculations of the cross sections of the 42.5 meV phonon as well as other phonons. In order to assess the model dependence of the calculated cross section we have implemented two different models, a simple nearest-neighbor force constant model and the model of Chaplot[28] which takes long-range Coulomb interactions into account. Details of the calculations are given in Appendix A. The latter model is more elaborate but involves a greater number of parameters, each of which carries some uncertainty. Since these models were constructed on the basis of light scattering

data (where $\mathbf{q}=0$), it is interesting in itself to test them against measured phonon eigenvectors at nonzero $\mathbf{q}$.

The calculations presented in Appendix A yield a set of phonon eigenvectors $\hat{\eta}(\mathbf{q})$ and dispersions $\omega_p(\mathbf{q})$, which can be used to calculate the cross section for phonon creation by nuclear neutron scattering per formula unit:

$$\frac{\partial^2\sigma}{\partial\Omega\,\partial E}=\frac{k_f}{k_i}\left(\sum_{\mathbf{d}} e^{-i\mathbf{q}\cdot\mathbf{d}}\frac{[\mathbf{Q}\cdot\hat{\eta}_{\mathbf{d}}(\mathbf{q})]e^{-W}\mathbf{d}^{(\mathbf{Q})}b_{\mathbf{d}}}{\sqrt{M_{\mathbf{d}}}}\right)^2 \times\frac{\hbar}{2\omega_p(\mathbf{q})}[1+n(\omega)]\delta[\hbar\omega-\hbar\omega_p(\mathbf{q})], \quad (2)$$

where k_i and k_f are the wave vectors of the incident and scattered neutrons, respectively, $\mathbf{Q}=\mathbf{k_f}-\mathbf{k_i}$ is the momentum transferred to the neutron, $\mathbf{q}$ is the reduced momentum measured from a reciprocal-lattice vector, and $b_{\mathbf{d}}$, $M_{\mathbf{d}}$, and $W_{\mathbf{d}}(\mathbf{Q})$ are the scattering length, mass, and Debye-Waller factor of the atom at basis site $\mathbf{d}$ in the unit cell, respectively. The Bose population factor $[1+n(\omega)]$ differs only insignificantly from 1 for $\hbar\omega=40$ meV in the temperature range of interest.

Figure 2 shows measurements of the scattering cross section at 41 meV which in the normal state is entirely dominated by scattering from a single phonon mode, the 42.5 meV oxygen vibration whose eigenvector is shown in the inset. (The energy resolution in most of our experiments was 8.3 meV full width at half maximum, and our numerical calculation confirms that in this energy window the cross sections of other phonons are significantly smaller than the one of the 42.5 meV mode at the $\mathbf{Q}$ points of interest.) The lines in the figure are predictions of the two lattice dynamical models, which obviously agree very well both with each other and with the experimental data. We can thus extract the cross section of this phonon mode from our data in a model-independent fashion.

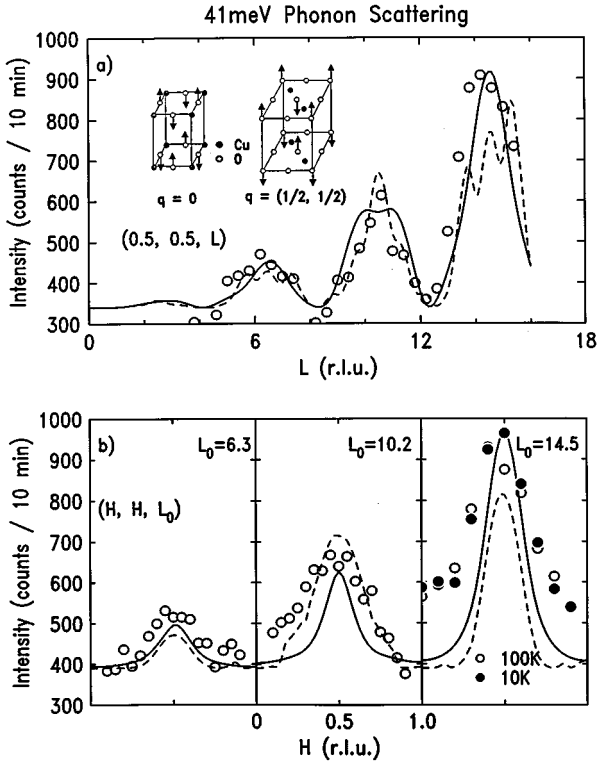

FIG. 2. Cross section of the 42.5 meV oxygen vibration, measured at $\hbar\omega=41$ meV and momentum transfers of the form (a) $\mathbf{Q}=(1/2,1/2,L)$ and (b) $\mathbf{Q}=(H,H,L_0)$ for different L_0. The solid line is the result of a calculation based on a nearest-neighbor force constant model. The broken line results from a calculation which includes long-range Coulomb forces. Only the background and the overall scale were adjusted to give the best fit to the data. The inset is the dominant contribution to the eigenvector predicted by both models.

In Ref. 9 we have shown that the 42.5 meV phonon and the 40 meV magnetic resonance can be separated by a judicious choice of the scattering geometry. The new geometry developed for this purpose is shown in Fig. 3. The data presented in Fig. 3 of Ref. 9 shows that in the zone specified by $\mathbf{Q}=(3/2,1/2,L)$ the magnetic intensity for $L=1.7$ and $T=10$ K is equal to the phonon intensity for $L=6.2$ and $T=100$ K. From Eq. (2) and the eigenvector of Fig. 2 we easily obtain for $\mathbf{Q}=(3/2,1/2,6.2)$

$$\frac{\partial^2\sigma}{\partial\Omega\,\partial E}=\frac{k_f}{k_i}\frac{\hbar b_{\mathrm{O}}^2 Q_\perp^2}{m_{\mathrm{O}}\omega_p(\mathbf{q})}\,\delta[\hbar\omega-\hbar\omega_p(\mathbf{q})], \quad (3)$$

where $Q_\perp=Lc^*=3.3$ Å^{-1} is the total momentum transfer perpendicular to the CuO_2 layers, and b_{O} and m_{O} are the scattering length and the mass of the oxygen atom, respectively. Since all of these quantities are known, the phonon cross section is completely specified. In addition to the c-axis motion of the in-plane oxygen, both models also predict small admixtures of other atomic motions for nonzero $\mathbf{q}$. However, these admixtures reduce the calculated cross section by less than 10% with respect to Eq. (3).

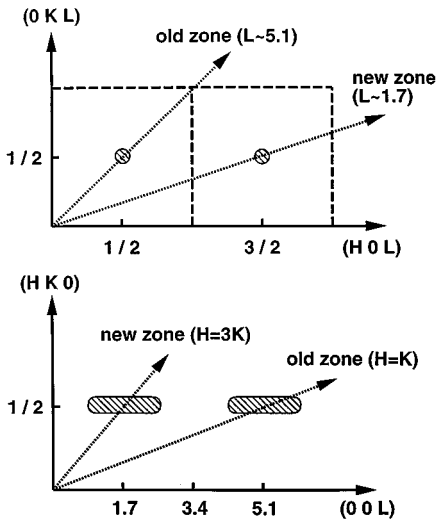

FIG. 3. New scattering geometry developed by Fong *et al.* (Ref. 9) in order to minimize phonon scattering as well as contamination by accidental Bragg scattering around $\hbar\omega=40$ meV. The hashed areas represent regions of strong inelastic magnetic scattering. The new geometry, where momentum transfers of the form $\mathbf{Q}=(3H,H,L)$ are in the scattering plane, is contrasted with the traditional geometry which uses momentum transfers of the form $\mathbf{Q}=(H,H,L)$.

The cross section for *magnetic* neutron scattering per formula unit can be written as

$$\frac{d^2\sigma}{d\Omega dE} = \frac{k_f}{k_i} f^2(\mathbf{Q}) e^{-2W(\mathbf{Q})} r_0^2 \frac{1}{4} (1+\hat{Q}_x^2)[1+n(\omega)] \times \chi''(\mathbf{q},\omega), \quad (4)$$

where the spin direction is $\hat{x}$, $r_0 = 5.4\times10^{-15}$ m, $f(\mathbf{Q})$ is the magnetic form factor, and $e^{-2W(\mathbf{Q})}$ is the Debye-Waller factor. Our units for the dynamical susceptibility $\chi''(\mathbf{q},\omega)$ are defined in Appendix B. Again, we have $1+n(\omega)\approx 1$. The polarization factor must be rotationally averaged, yielding $(1+\langle \hat{Q}_x^2 \rangle)=4/3$. We have measured the magnetic form factor for $\mathbf{Q}=(3/2,1/2,1.7)$ in $YBa_2Cu_3O_{6.2}$ and obtain $f^2(\mathbf{Q})=0.45$, consistent with previous investigations.[2] As both the localized electrons in the antiferromagnetic insulator and the doped holes in the superconductor are known to reside in the same hybridized $d_{x^2-y^2}-p_x/p_y$ orbitals, the form factor is not expected to be appreciably different in $YBa_2Cu_3O_7$.

In the next section we will show that the magnetic resonance is well described by

$$\chi''_{\rm res}(\mathbf{q},\omega) = A(T) e^{-(\mathbf{q}_\parallel - \mathbf{q}_{\parallel 0})^2/\kappa^2} \sin^2(\pi Q_\perp z_{\rm Cu} c) \times \delta(\hbar\omega - 40\ \text{meV}), \quad (5)$$

where $\kappa = 0.23$ Å^{-1} (corresponding to a HWHM of 0.19 Å^{-1}), $z_{\rm Cu}c = (3.4\ \text{r.l.u})^{-1}$ is the distance of nearest-neighbor copper atoms within a bilayer, and $A(T)$ is the energy-integrated spectral weight we wish to determine in absolute units. Since both the phonon and the resonance are resolution limited in energy, their amplitudes can be directly compared without a resolution deconvolution. From Eqs. (2)–(5) we obtain

$$A(T=10\ \text{K}) = \int d(\hbar\omega)\chi''_{\rm res}(\mathbf{q}_{\parallel 0},\omega) = 0.51\pm0.1. \quad (6)$$

The error arises mostly from an uncertainty in the determination of the background level. Equivalently, we may use the Kramers-Kronig transformation to write the real part of the susceptibility associated with the resonance as

$$\chi'_{\rm res}(\mathbf{q}_{\parallel 0},0) = \frac{2}{\pi} \frac{\int d(\hbar\omega)\chi''_{\rm res}(\mathbf{q}_{\parallel 0},\omega)}{40\ \text{meV}} = (8\pm2)\ \frac{\text{states}}{\text{eV}}. \quad (7)$$

A similar analysis was carried out along $\mathbf{Q}=(1/2,1/2,L)$, where the resonance can be isolated by taking temperature subtractions. The result was identical to within our experimental error.

B. Antiferromagnetic spin waves

In another, independent scheme to obtain the cross section in absolute units, we compare the cross section of the 40 meV magnetic resonance in the superconducting state of our $YBa_2Cu_3O_7$ crystal to the cross section of antiferromagnetic spin waves measured in the same crystal after reduction to $YBa_2Cu_3O_{6.2}$. Again, in order to avoid contamination by phonon scattering,[9,10] most of the data were taken near the (3/2,1/2,1.7) point in reciprocal space. Limited data were also collected near (1/2,1/2,5.2).

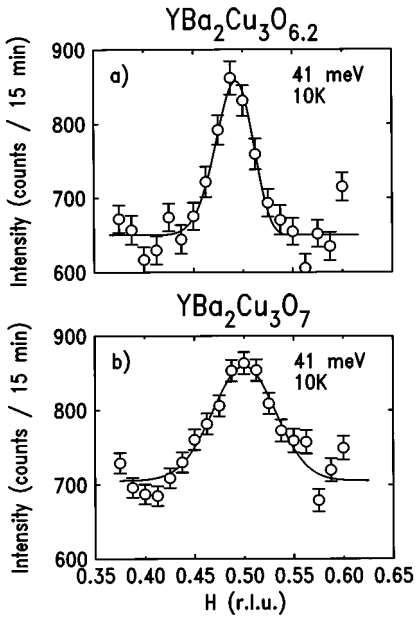

FIG. 4. Constant-energy scans at $\hbar\omega=41$ meV with $\mathbf{Q}=(3H,H,-1.7)$ on the same sample in oxygenation states (a) $YBa_2Cu_3O_{6.2}$ and (b) $YBa_2Cu_3O_7$, under identical experimental conditions. The lines are the results of convolutions of Eqs. (8) and (5), respectively, with the experimental resolution function.

The dynamical susceptibility of antiferromagnetic $YBa_2Cu_3O_{6+\delta}$ differs from the well-known[29] susceptibility of a two-sublattice, large-spin antiferromagnet in two respects: First, due to the bilayer structure the spin-wave spectrum is split into acoustic and optical spin-wave modes.[1] At $\hbar\omega=40$ meV only acoustic spin waves are observed. Their cross section contains a structure factor $2\sin^2(\pi Q_\perp z_{\rm Cu} c)$. Second, quantum fluctuations of the spins $-1/2$ renormalize both the dynamical susceptibility and the spin-wave dispersions by factors of $Z_\chi=0.51$ and $Z_c=1.18$, respectively.[30] The susceptibility of antiferromagnetic $YBa_2Cu_3O_{6+\delta}$ can thus be written as

$$\chi''(\mathbf{q},\omega) = 4SZ_\chi Z_c \frac{1+\gamma(\mathbf{q}_\parallel)}{\sqrt{1-\gamma^2(\mathbf{q}_\parallel)}} \sin^2(\pi Q_\perp z_{\rm Cu} c) \times \delta[\hbar\omega - 4SZ_c J\sqrt{1-\gamma^2(\mathbf{q}_\parallel)}], \quad (8)$$

where

$$\gamma(\mathbf{q}_\parallel) = \tfrac{1}{2}\,[\cos(q_x a)+\cos(q_y a)] \quad (9)$$

and $J=100$ meV.[2] In deriving Eq. (8) we have used the fact that $\hbar\omega=40$ meV much exceeds the anisotropy gap in the spin-wave spectrum,[1] so that spin-wave modes polarized within and out of the CuO_2 layers contribute equally to the susceptibility.

Figure 4 shows constant-energy scans at $\hbar\omega=41$ meV taken at the maximum of the $\sin^2$ structure factor [$\mathbf{Q}=(3/2,1/2,1.7)$] for both $YBa_2Cu_3O_{6.2}$ and $YBa_2Cu_3O_7$ at $T=10$ K, under identical experimental conditions. The spectral weight is obviously comparable in both cases. Because of the different functional forms of Eqs. (8) and (5), a numerical convolution with the resolution function must be car-

ried out in order to compare both susceptibilities quantitatively. The results of such convolutions are shown in the solid lines of Fig. 4. Only the background and the amplitudes were adjusted to give the best fit to the data.

After the amplitudes are corrected for the polarization factor in Eq. (4) (which implies a rotational average for $YBa_2Cu_3O_7$ and an average over the twin domains in $YBa_2Cu_3O_{6.2}$) we obtain

$$A(T=10\ \ K)=\int d(\hbar\omega)\chi''_{\rm res}(\mathbf{q}_{\|0},\omega)=0.54\pm0.1. \quad (10)$$

Here the dominant contribution to the error is the mosaic structure of our sample, which affects the deconvolution of the data of Fig. 4 to some degree. The excellent agreement of the spectral weights obtained by both methods of normalization [Eqs. (6) and (10)] gives us confidence in the accuracy of this analysis. Both methods are not entirely redundant, however, as the susceptibility renormalization factor Z_χ has thus far not been measured directly in $YBa_2Cu_3O_{6+\delta}$.[31] Within our errors, the measured value is consistent with the one predicted by spin-wave theory.

V. EXPERIMENTAL RESULTS

A. Background

All neutron-scattering experiments thus far reported on $YBa_2Cu_3O_7$ have suffered from signal-to-background ratios less than one. In order to measure the magnetic cross section reliably, extreme care must therefore be taken to subtract the background properly. In this section we give a discussion of the various relevant contributions to the background in both polarized and unpolarized beam experiments. We emphasize possible systematic errors, in particular in polarized beam experiments.

The background in an unpolarized beam experiment is dominated by scattering from phonons, both through one-phonon and through multiphonon events. As we have already demonstrated for a specific case in the previous section, single-phonon events give rise to distinct features in the cross section, which can be identified through Eq. (2) if a lattice dynamical calculation is available. This ''footprint'' is relatively straightforward to identify for the 42.5 meV phonon, as the eigenvector is quite simple and the mode is nondispersive. Surprisingly, the dynamical structure factor of this phonon resembles that of a low-energy spin wave in antiferromagnetic $YBa_2Cu_3O_{6+\delta}$. Another, very broad feature centered around $\mathbf{q}_{\|0}$ and $\hbar\omega=30$ meV which also resembles such a magnetic excitation was observed by Rossat-Mignod *et al.*[5] We have confirmed that in this energy range the cross section exhibits a broad peak centered around $\mathbf{q}=(1/2,1/2)$. Typical data are shown in Fig. 5(a) for $\hbar\omega=35$ meV. However, the data of Fig. 5(b) demonstrate that this feature also arises from phonon scattering, as its cross section increases dramatically with increasing $\mathbf{Q}$. (This conclusion was reached previously[7] on the basis of polarized-beam experiments.) We can again compare the measured cross section with the prediction of our lattice dynamical calculation, shown in the solid line of Fig. 5(a). In order to obtain this line we simply added the cross sections of the five phonons which were found to be in the resolution volume at the center

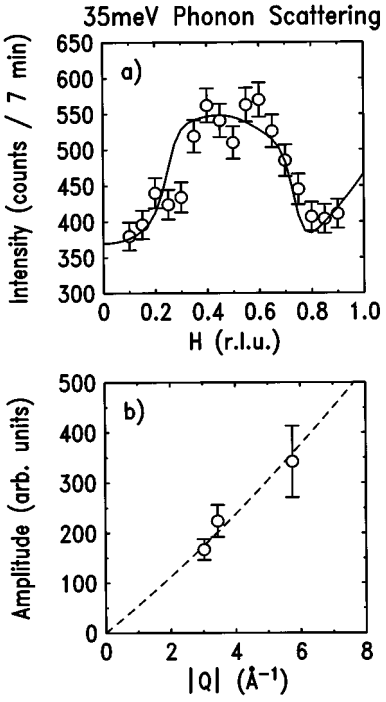

FIG. 5. (a) Constant-energy scan at $\hbar\omega=35$ meV with $\mathbf{Q}=(H,H,-5.2)$ taken at $T=100$ K. The solid line is the prediction of a lattice dynamical calculation, as discussed in the text. (b) Amplitude of the peak in (a), measured at $\mathbf{Q}=(1/2,1/2,-5.2)$, $\mathbf{Q}=(3/2,3/2,0)$, and $\mathbf{Q}=(5/2,5/2,0)$. The dashed line is a guide to the eye. The increase of the amplitude with increasing $|\mathbf{Q}|$ demonstrates the lattice vibrational origin of the signal.

of the scan, without attempting to weight their respective contributions according to their overlap with the resolution ellipsoid, or to correct for phonon dispersion. (Note that the 42.5 meV phonon does not contribute to the 35 meV cross section.) The same analysis was carried out for $\hbar\omega=30$ meV and at $\hbar\omega=41$ meV (Fig. 2), with similar results. Despite this approximate treatment the phonon calculation again captures the behavior of the cross section very well, in particular the broad peak around $\mathbf{q}_{\|}=(1/2,1/2)$.

We have thus plausibly identified the origin of the features observed in previous unpolarized-beam experiments above T_c as arising from single-phonon scattering. In particular, our analysis provides a good explanation of the early data of Rossat-Mignod and collaborators on $YBa_2Cu_3O_7$. Most of the remaining $\mathbf{q}$-independent background in Figs. 2 and 5(a) presumably arises from multiphonon scattering. In contrast to the distinct features generated by one-phonon scattering, multiphonon scattering gives rise to a broad and featureless background, as for any given momentum transfer $\mathbf{Q}$ and energy transfer $\hbar\omega$ energy and momentum conservation can be satisfied by many different multiphonon events. A featureless magnetic cross section generated, for example, by the particle-hole continuum of a metal cannot be separated from the multiphonon background and is thus not measurable by unpolarized neutron scattering.

Another normal-state feature observed by Mook *et al.* in polarized-beam experiments is a sharp peak at 41 meV in the spin-flip channel [Fig. 1(a) of Ref. 7 and Fig. 2 of Ref. 8]. Though small, this peak appeared to contradict our assertion

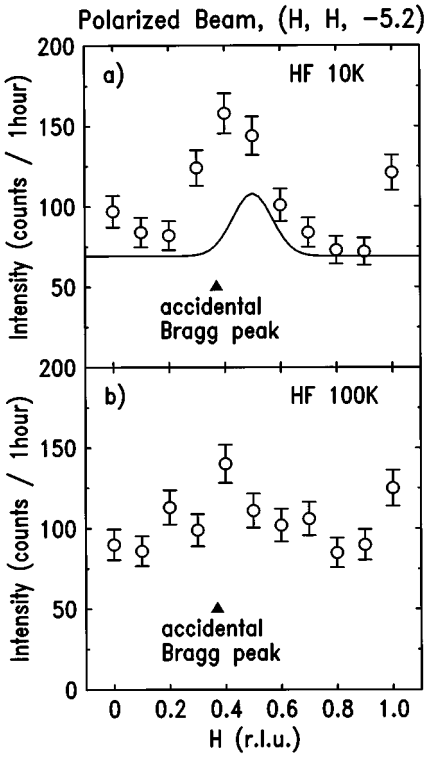

FIG. 6. Horizontal-field polarized beam measurements (a) below and (b) above T_c, in the geometry used by Mook *et al.* (Ref. 7). The accidental Bragg peak, here observed at $H=0.4$, occurs at $H=0.5$ when the same final energy as in Ref. 7 is used. The solid line is the signal of the magnetic resonance below T_c expected on the basis of unpolarized beam experiments.

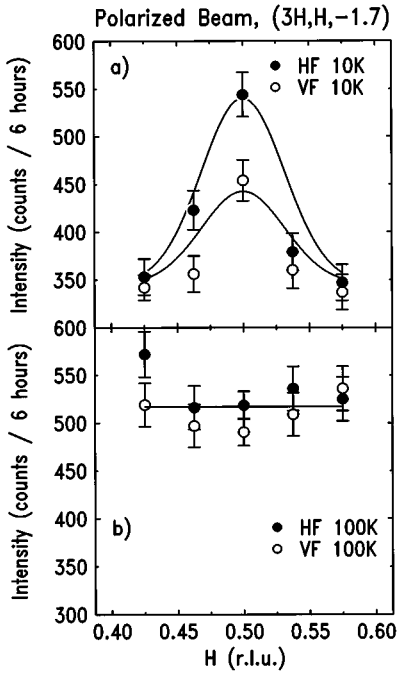

FIG. 7. Horizontal-field (HF) and vertical-field (VF) polarized beam measurements in the new geometry (Fig. 3), taken (a) below and (b) above T_c. The lines in (a) are the signal expected on the basis of unpolarized beam experiments, with only the background adjusted. The data in (a) and (b) were taken under identical conditions, but in separate runs with somewhat different background levels.

that the 41 meV feature in the normal state arises from phonon scattering.[9] We thus attempted to reproduce the data of Mook *et al.*

Figure 6 shows a polarized-beam (HF) scan in the zone near the (1/2,1/2,5.2) point used by Mook *et al.* The **q** scan clearly shows a sharp maximum near $\mathbf{q}_{\parallel}=(1/2,1/2)$, and an energy scan (not shown) shows a peak near 41 meV, in agreement with the data of Mook *et al.* However, we were able to conclusively demonstrate a spurious origin of this normal-state peak: Although it nominally appears in the ''spin-flip'' channel, it actually arises from a *nuclear* scattering event. At the sample orientation corresponding to the point of maximum intensity the sample accidentally satisfies the Bragg condition for a nuclear reflection, and the neutrons are elastically scattered. As the neutrons arrive at the analyzer, they do not satisfy its Bragg condition and must undergo weaker (inelastic, incoherent) scattering events to be deflected into the detector. The large cross section for nuclear Bragg scattering at the sample compensates for the weakness of the scattering from the analyzer. Such ''accidental Bragg scattering'' is well known and can be identified through simple tests such as repeating the scan with the analyzer set at the incident energy.

These processes are somewhat more subtle in polarized beam experiments as the above scenario does not account for the apparent spin flip of the neutron. This is explained, however, by the fact that the flipper behind the sample is tuned to a specific energy and does not efficiently flip the spin of elastically scattered neutrons. What is detected are actually neutrons of the original spin direction which are simply transmitted by the flipper. This spurious process thus provides the explanation for the sharp peak observed by Mook *et al.*[7,8] above T_c and removes the apparent discrepancy with our unpolarized beam experiments. The fact that the spurious peak appears even in HF-VF measurements at $T=100$ K (Ref. 8) is presumably due to different and relatively low flipping ratios for HF and VF in Refs. 7 and 8. This illustrates that at the very low signal levels under study the background subtraction in polarized beam experiments is nontrivial.

B. Magnetic resonance peak

We have taken several precautions to avoid such spurious events in our own polarized beam experiments. Our measurements were taken in the zone near the (3/2,1/2,1.7) point developed in Ref. 9. This zone has several advantages: First, phonon scattering near 40 meV is suppressed, which is important for unpolarized beam experiments but only of minor relevance to polarized beam experiments. More importantly, in contrast to (H,H) the $(3H,H)$ direction is a low symmetry direction where fewer accidental Bragg scattering events occur. We verified the absence of such contamination explicitly by conducting the standard tests.

Figure 7(a) shows raw (uncorrected) polarized beam data taken in this zone in horizontal and vertical guide fields at $T=10$ K. The flipper in on, and the scattering intensity is described by Eq. (1). A substantial background (consisting of

several contributions as discussed in Secs. III and V A) is apparent in the data. However, since we have carried out measurements in both horizontal and in vertical field, the precise origin of the background is irrelevant. The magnetic contribution to the signal can simply be obtained by subtracting the HF and VF data and multiplying by 2. Figure 7(a) once again confirms the magnetic origin of the resonance in the superconducting state,[5,7,9,10] as there is a clear magnetic signal outside the statistical error at $\mathbf{q}_{\|}=(3/2,1/2)$. The data also show that near the boundary of the magnetic Brillouin zone HF and VF signals are identical, and the magnetic signal is zero to within our experimental error. Figure 7(b) in the normal state also shows a null result to within the statistical error. This will be discussed in more detail in Sec V C.

We can now combine our determination of the absolute intensity scale and the background and study the behavior of the resonance as a function of temperature. This is best done with unpolarized neutrons as the intensity decreases markedly at high temperatures, and the counting time for polarized beam scans becomes prohibitively long. As we now know that the resonance disappears in the normal state and the phonon intensity at 40 meV is temperature independent [Fig. 2(b)], the resonance intensity is given by taking the difference of data taken below T_c and data taken at $T=100$ K. As a crosscheck we corrected such a difference scan for the reduced reflectivity and the loss of one spin polarization direction at the Heusler monochromator and analyzer, fitted it to a Gaussian and compared the result to the polarized beam data [solid line in Fig. 7(a)]. The only adjustable parameter in this comparison is the background. The result obviously justifies our subtraction procedure. Incidentally, Fig. 6(a) shows that the same subtraction procedure does not work in the $(H,H,5.2)$ zone due to contamination by accidental Bragg scattering.

Typical unpolarized beam data at various temperatures are shown in Fig. 8. At all temperatures they are well described by resolution-limited Gaussians, which means that the intrinsic width of the resonance peak can be at most ~ 3 meV.[32] (A larger intrinsic width would have been reflected in an observed energy width larger than the width of the resolution function, which was as small as 5.5 meV in some cases.) In the fits the resonance width was thus kept fixed at the instrumental resolution, and the only two fitting parameters, the amplitude and the position of the resonance, are shown in Fig. 9 as a function of temperature. With increasing temperature the resonance spectral weight continuously decreases from $\int d(\hbar\omega)\chi''_{\rm res}(\mathbf{q}_{\|0},\omega)=0.5$ at 10 K and approaches zero (to within our experimental error) at a temperature around 90 K, consistent with a disappearance of the resonance at or near $T_c=93$ K. The temperature dependence of the resonance below T_c is consistent with previous studies.[7,11] Up to $T=75$ K $(=0.8T_c)$ the resonance energy remains constant to within the experimental accuracy (~ 2 meV at $T=75$ K).

One of the characteristic signatures of the 40 meV resonance is its sinusoidal modulation as a function of $Q_\perp$ [Eq. (5)]. An important question is whether the intensity truly goes to zero at the minima of the $\sin^2$ modulation, or whether there is any sign of magnetic scattering at these points. A scan of the modulation taken with higher counting statistics than before is shown in Fig. 10. It is apparent that we cannot

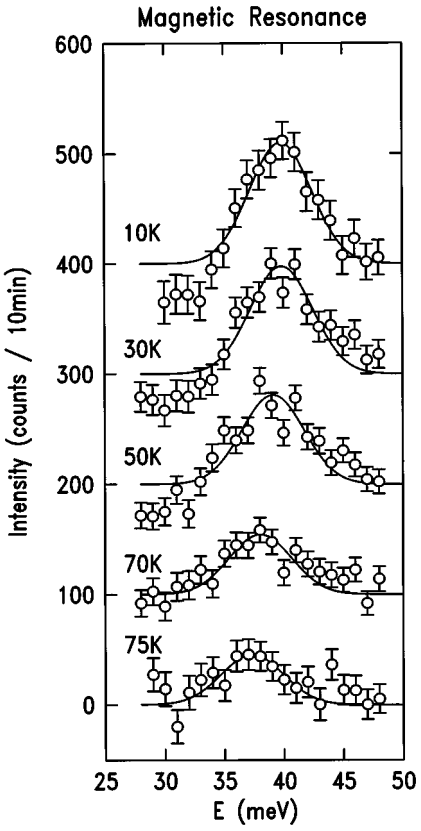

FIG. 8. Unpolarized beam, constant-**Q** data [$\mathbf{Q}=(3/2,1/2,-1.7)$] of the 40 meV magnetic resonance obtained by subtracting the signal below T_c from the $T=100$ K background. The lines are fits to Gaussians, as described in the text. For clarity successive scans are offset by 100.

rule out the presence of a $\cos^2$ modulation of amplitude less than $\sim 30\%$ of that of the $\sin^2$ modulation at $\hbar\omega=40$ meV. We have also conducted extensive surveys of the scattering cross section as a function of both **q** and ω with $Q_\perp$ fixed at

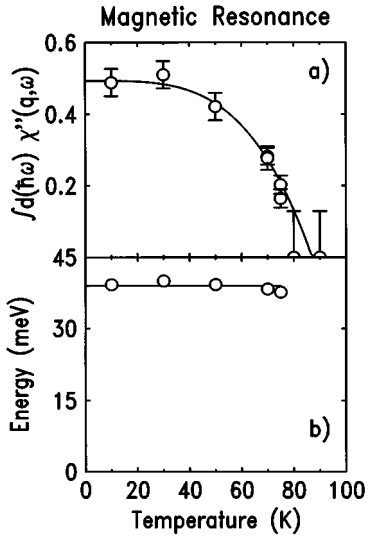

FIG. 9. (a) Absolute spectral weight and (b) energy of the resonance obtained by fits to the data of Fig. 8. The error bars in (a) do not include the normalization error. The lines are guides to the eye.

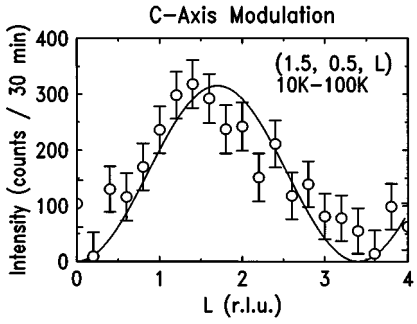

FIG. 10. Constant-energy scan along $\mathbf{Q}=(3/2,1/2,L)$ at $\hbar\omega=41$ meV. Data at $T=10$ K were subtracted from the $T=100$ K background. The line is the expression $\sin^2(\pi z_{\mathrm{Cu}} Q_\perp c)$ with $Q_\perp = Lc^*$.

the minima of the $\sin^2$ modulation, but found no temperature-dependent signal outside of our experimental error.

C. Normal-state spin susceptibility

Figure 10 shows the raw data obtained in a **q** scan at $\hbar\omega=41$ meV in the normal state ($T=100$ K). Data taken in several runs in the normal state are compiled in Fig. 11 as a function of energy and compared to data in the superconducting state taken under the same experimental conditions. The data at $\hbar\omega=40$ meV, where we have taken constant-energy in addition to constant-**Q** scans, were extracted both by taking HF-VF differences (circles in Fig. 11) and by subtracting a weighted average of the signal at the two borders of the HF scan in Fig. 7(a) (and a similar scan not shown) from the signal at the peak (squares in Fig. 11). The latter method could be associated with significant systematic errors only if there were a significant **q**-independent magnetic contribution, or if the nonmagnetic contribution to the HF signal [Eq. (1)] showed a **q**-dependent structure around $\mathbf{q}=\mathbf{q}_{\|0}$. Inspection of the scans in Fig. 10 shows that this is not the case.

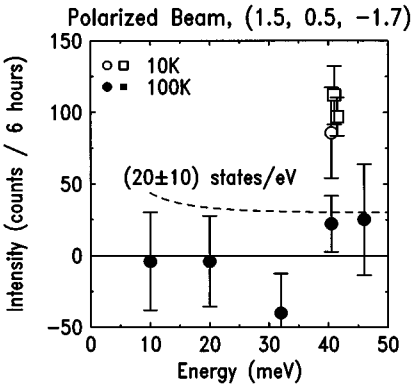

FIG. 11. Polarized-beam data in the superconducting state (open symbols) and normal state (closed symbols) at $\mathbf{q}=\mathbf{q}_{\|0}$. The circles were determined by HF-VF subtractions, the squares result from **q** scans such as the ones in Fig. 7, as discussed in the text. The dashed line, corresponding to $\chi''(\mathbf{q}_{\|0},\omega)=20\pm10$ states/eV, is an upper bound on the normal-state ($T=100$ K) susceptibility for $10\leqslant\hbar\omega\leqslant40$ meV. (The line is not straight due to the Bose population factor in the magnetic cross section.)

None of the normal-state data points shows a signal significantly outside the statistical error bar. We wish to state the implications of this observation carefully. In particular, we reiterate[9] at the outset that our data *do not* imply that the dynamical susceptibility *vanishes* in the normal state, which would be theoretically nonsensical and impossible to prove with any experiment. Rather, we can use our absolute intensity scale to put a quantitative upper bound on the dynamical spin susceptibility in the normal state, $\chi_n''(\mathbf{q}_{\|0},\omega)$. To this end we assume that this quantity is only weakly energy dependent in the range $10\leqslant\hbar\omega\leqslant40$ meV, as predicted by many models. For simplicity we consider an energy independent $\chi_n''(\mathbf{q}_{\|0},\omega)$.

A straightforward statistical analysis of the data of Fig. 11 reveals that at $T=100$ K in this energy range an energy-independent count rate specified by the dashed line can be ruled out with $>95\%$ confidence. For an ω-independent susceptibility the count rate is proportional to $\chi_n''(\mathbf{q}_{\|0},\omega)\Delta(\hbar\omega)$, where $\Delta(\hbar\omega)=8.3$ meV is the energy resolution (FWHM). By normalizing to the resolution-limited resonance signal in the superconducting state [whose count rate is proportional to $\int d(\hbar\omega)\chi''_{\mathrm{res}}(\mathbf{q}_{\|0},\omega)$] we obtain $\chi_n''(\mathbf{q}_{\|0},\omega)=(20\pm10)$ states/eV as the susceptibility corresponding to the dashed line. Factors contributing to this very conservative estimate of the error bar are the normalization error, the statistical error of the 10 K signal and a systematic error associated with calculating the energy resolution. A very conservative upper bound on an energy-independent normal-state susceptibility at $\mathbf{q}=\mathbf{q}_{\|0}$ is therefore 30 states/eV in the energy range $10\leqslant\hbar\omega\leqslant40$ meV. Models which predict a strong energy dependence of $\chi_n''(\mathbf{q}_{\|0},\omega)$ would generally be less constrained by our data, with details depending on the specific model. Above $\hbar\omega=40$ meV kinematic constraints and interference with the unscattered beam make polarized beam experiments difficult in the geometry we have chosen (hence the large error bar at $\hbar\omega=46$ meV).

As discussed in Sec. III, the only systematic error in our HF-VF measurements is the slight difference in HF and VF flipping ratios due to fringing effects in the guide fields. Because of our high overall beam polarization, systematic errors due this effect are at most $\sim10\%$ of the statistical error bar for the data in Fig. 11, but would be much more relevant if the counting time were significantly increased in order to decrease the statistical error, or for significantly smaller overall beam polarizations.[7]

VI. DISCUSSION AND CONCLUSION

In addition to neutron-scattering experiments, much information about the spin dynamics of $YBa_2Cu_3O_7$ has been extracted from measurements of the nuclear magnetic relaxation rates T_1 and T_2. According to the standard interpretation of these data,[33] $1/T_1T=\lim_{\omega\to0}\Sigma_{\mathbf{q}}F(\mathbf{q})\chi''(\mathbf{q},\omega)$, where the form factor $F(\mathbf{q})$ is peaked at $\mathbf{q}=\mathbf{q}_{\|0}$ for the copper nucleus. Since none of our data were taken in the low-ω regime, a direct comparison between our data and copper T_1 NMR data on $YBa_2Cu_3O_7$ is not possible. However, Millis and Monien[33] have devised a phenomenological model which is consistent with an extensive set of T_1 and T_2 data. Although the NMR directly only measures the zero-frequency spin dynamics, the temperature dependence of

these quantities allows some conclusions about the energy scales associated with the spin excitations in $YBa_2Cu_3O_7$. The analysis of Refs. 33 and 18 has resulted in a maximum susceptibility of $\chi''(\mathbf{q}_{\|0},\omega_{SF})\sim 10-20$ states/eV (for the appropriate unit conversions, see Appendix B), where $\hbar\omega_{SF}\sim 20-40$ meV is the characteristic energy of the spin excitation spectrum. The maximum susceptibility extracted (with significant uncertainty) from NMR measurements is thus below our upper bound, and more sensitive neutron measurements are needed to provide a strong independent test of current theoretical interpretations of $YBa_2Cu_3O_7$ NMR data.

Our normal-state data are at variance with the data of Mook *et al.*[7] who under experimental conditions similar to ours report an energy independent continuum above T_c, with an amplitude of about 1/2 of the resonance amplitude in the superconducting state. We have also found no evidence for such a continuum in the superconducting state.[7] These ''continua'' may be artefacts of the background subtraction of Ref. 7, but small differences in the oxygen content could also play a role. On the other hand, our data are consistent with recent data of Bourges *et al.*,[11] who have found weak evidence for normal-state magnetic excitations with an amplitude $\sim 1/10$ of the resonance amplitude in the superconducting state. The overall scale of the $\chi''(\mathbf{q}_{\|0},\omega)$ is also consistent with measurements on $La_{1.86}Sr_{0.14}CuO_4$.[27,34]

The 40 meV resonance is characterized by the following experimental signatures: (a) presence in the superconducting state *only*; (b) very small width in energy ($\leqslant 3$ meV FWHM); (c) moderately sharp peak in $\mathbf{q}_{\|}$; (d) sinusoidal intensity modulation as a function of $Q_{\perp}$; (e) strong temperature dependence of the resonance intensity beginning at $T\sim 0.5T_c$; (f) weak or absent temperature dependence of the resonance energy at least up to $T=0.8T_c$; and (g) low-temperature energy-integrated spectral weight of ~ 0.5 in absolute units.

As our theoretical understanding of the 40 meV resonance is still in a stage of rapid development, a detailed comparison of these features to the predictions of the different models would be premature at this point. Some qualitative observations can nevertheless be made.

First, all theoretical treatments[9,12–14,16–18] of the 40 meV resonance stress that in order to reproduce the sharpness of the resonance in both $\mathbf{q}_{\|}$ and ω a strong enhancement of $\chi''(\mathbf{q},\omega)$ over the noninteracting Lindhard susceptibility must be invoked. The present measurements on an absolute scale underscore this point: Susceptibilities of the order of the band susceptibility [$\chi''(\mathbf{q},\omega)\sim 1$ state/eV] would be immeasurably small. Quantitatively, none of the presently published theoretical predictions have been made in absolute units, but efforts to this end are presently underway.[35] Preliminary results indicate that the absolute spectral weight of the resonance will provide a strong additional constraint on its theoretical interpretation. Further constraints will come from a comparison of our data to measurements of the superconducting energy gap as a function of temperature in $YBa_2Cu_3O_7$. Photoemission experiments on $Bi_2Sr_2CaCu_2O_{8+\delta}$ (Ref. 36) have shown that this quantity is energy independent within the measurement error at least up to $T\sim 0.8T_c$.

Even on a qualitative level, an interpretation of the 40 meV resonance in the superconducting state as a spin-wave-like excitation across a ''spin gap''[18] appears inconsistent with our data, as we find no evidence for the dispersing spin wave branch starting at $\hbar\omega=40$ meV which is implied by this model. In fact, a $\mathbf{q}$ scan through $\mathbf{q}_{\|0}$ at $\hbar\omega=45$ meV shows no signal above the background level. There is thus no obvious relation between the 40 meV resonance and the ''spin-gap'' phenomenon.

In summary, we have demonstrated a nonmagnetic origin of all features in the normal-state cross section $YBa_2Cu_3O_7$ previously associated with strong magnetic fluctuations. Of course, as any metal $YBa_2Cu_3O_7$ is certainly expected to allow low-energy spin-flip excitations. However, only an upper bound of 30 states/eV could be established for the resulting normal-state dynamical susceptibility for $\mathbf{q}=\mathbf{q}_{\|0}$ and $10\leqslant\hbar\omega\leqslant 40$ meV, and below this level the functional form of $\chi''(\mathbf{q},\omega)$ in this energy range must hence be regarded as unknown. The upper bound derives from high-quality polarized-beam experiments (horizontal-minus-vertical field, high beam polarizations, no contamination by elastic scattering) and is not in conflict with current phenomenological interpretations of NMR data.

Based on this thorough characterization of the background we were able to determine the functional form, spectral weight, and temperature dependence of the susceptibility arising from the 40 meV resonance in the superconducting state of $YBa_2Cu_3O_7$ in detail. The data presented here provide a solid basis for a theoretical interpretation of this phenomenon.

ACKNOWLEDGMENTS

We thank the Brookhaven neutron scattering group, in particular G. Shirane, J. D. Axe, S. M. Shapiro, B. J. Sternlieb, and J. M. Tranquada for their hospitality and many helpful discussions. We are grateful to P. Bourges for his measurement of the Néel temperature. We have also greatly benefited from fruitful interactions with many others, especially P. W. Anderson, K. Levin, I. I. Mazin, A. J. Millis, H. Monien, V. M. Yakoveno, and S. C. Zhang. The work at Princeton University was supported by the MRSEC program of the National Science Foundation under Grant No. DMR94-00362, and by the Packard Foundation. The work at Brookhaven was supported by the U.S. Department of Energy under Contract No. DE-ACO2-76CH00016.

APPENDIX A

Several models of the lattice dynamics of $YBa_2Cu_3O_7$ have been published,[37,28,38,29,32,40] but details of the rather involved calculations have not been given. Despite their usefulness in identifying features in neutron spectra which arise from phonon scattering, such calculations have thus far not been widely employed. The following account will enable others to reproduce our calculations without a major effort.

The tenet of obtaining the eigenmodes of a lattice can be summarized as follows. The potential energy of a lattice is given by

$$\Phi(\{\mathbf{r}_{ld}\})=\frac{1}{2}\left[\sum_{ll'}\sum_{dd'}\right]'\Phi_{dd'}(|\mathbf{r}_{ld}-\mathbf{r}_{l'd'}|), \qquad \text{(A1)}$$

where l, d, and $\Phi_{dd'}$ are the cell number, the constituent atom, and the two-body interaction, respectively. The prime at the sum means $(l,d)\neq(l',d')$. Φ's first derivative is assumed to vanish for a stable lattice. Its second derivatives are given by

$$\frac{\partial^2\Phi}{\partial r_{ld\alpha}\partial r_{l'd'\alpha'}}=\frac{\partial^2\Phi_{dd'}(|\mathbf{r}_{ld}-\mathbf{r}_{l'd'}|)}{\partial r_{ld\alpha}\partial r_{l'd'\alpha'}}$$

$$=-\frac{\partial^2\Phi_{dd'}(|\mathbf{r}_{ld}-\mathbf{r}_{l'd'}|)}{\partial r_{ld\alpha}\partial r_{ld\alpha'}},\quad (l,d)\neq(l',d'),$$

$$\frac{\partial^2\Phi}{\partial r_{ld\alpha}\partial r_{ld\alpha'}}=\left[\sum_{l'}\sum_{d'}\right]'\frac{\partial^2\Phi_{dd'}(|\mathbf{r}_{ld}-\mathbf{r}_{l'd'}|)}{\partial r_{ld\alpha}\partial r_{ld\alpha'}}. \quad \text{(A2)}$$

α denotes the spatial components (x,y,z). Let $u_{ld\alpha}=r_{ld\alpha}-\tau_{ld\alpha}$ (eq.). Then the force equations read

$$m_d\ddot{u}_{ld\alpha}=-\sum_{\alpha'}\left[\sum_{l'd'}{}'\frac{\partial^2\Phi_{dd'}(|\mathbf{r}_{ld}-\mathbf{r}_{l'd'}|)}{\partial r_{ld\alpha}\partial r_{ld\alpha'}}\right]\times u_{ld\alpha'}$$

$$+\sum_{\alpha'}\sum_{l'd'}{}'\frac{\partial^2\Phi_{dd'}(|\mathbf{r}_{ld}-\mathbf{r}_{l'd'}|)}{\partial r_{ld\alpha}\partial r_{ld\alpha'}}\times u_{l'd'\alpha'}. \quad \text{(A3)}$$

By the usual ansatz, i.e., $u_{ld\alpha}=u_{d\alpha}e^{-i\omega t}e^{2\pi i\mathbf{k}\cdot\boldsymbol{l}}$, they become

$$-m_d\omega^2u_{d\alpha}=\sum_{d'\alpha'}\begin{bmatrix}d & d'\\ \alpha & \alpha'\end{bmatrix}u_{d'\alpha'}, \quad \text{(A4)}$$

where we have adopted the notation of Kellermann:[39]

$$\begin{bmatrix}d & d'\\ \alpha & \alpha'\end{bmatrix}=\sum_{l'}\frac{\partial^2\Phi_{dd'}(|\mathbf{r}_d-\mathbf{r}_{l'd'}|)}{\partial r_{d\alpha}\partial r_{d\alpha'}}e^{2\pi i\mathbf{k}\cdot\boldsymbol{l}'},\quad d\neq d';$$

$$\begin{bmatrix}d & d\\ \alpha & \alpha'\end{bmatrix}=\sum_{l'\neq 0}\frac{\partial^2\Phi_{dd}(|\mathbf{r}_d-\mathbf{r}_{l'd}|)}{\partial r_{d\alpha}\partial r_{d\alpha'}}(e^{2\pi i\mathbf{k}\cdot\boldsymbol{l}'}-1)$$

$$-\sum_{d'\neq d}\sum_{l'}\frac{\partial^2\Phi_{dd'}(|\mathbf{r}_d-\mathbf{r}_{l'd'}|)}{\partial r_{d\alpha}\partial r_{d\alpha'}}.$$

In this form, the force balance condition is easily seen:

$$\sum_{d'}\begin{bmatrix}d & d'\\ \alpha & \alpha'\end{bmatrix}_{\mathbf{k}=0}=0. \quad \text{(A5)}$$

With the formalism above, specializations can be readily made by inserting the appropriate two-body interaction. For the nearest-neighbor force constants model the interaction is

$$\Phi_{dd'}(|\mathbf{r}_d-\mathbf{r}_{l'd'}|)=\frac{1}{2}c_{dd'}(|\mathbf{r}_d-\mathbf{r}_{l'd'}|-l_{dd'})^2. \quad \text{(A6)}$$

In our calculations, we adopted the spring constants used by Bates and Eldridge,[37] and then adjusted them so that the $\mathbf{k}=0$ eigenvectors fit more closely to the currently available Raman scattering results.[40] Our spring constants are given in Table I. We also followed Bates *et al.*[37] to include a torsional spring on the bilayer to take the buckling of the CuO_2 layers into account. The evaluation of the matrix elements is straightforward after this point and numerical methods to find the eigenvalues and vectors are well known.

TABLE I. Parameters used in our nearest-neighbor force constant model. The notation follows Bates and Eldridge (Ref. 37).

Force constant	Bond type	Value (J m^{-2})
$f1$	Cu(1)-O(1)	100
$f2$	Cu(1)-O(2)	140
$f3$	Cu(2)-O(3)	80
$f4$	Cu(2)-O(4)	80
$f4$	Cu(2)-O(4)	80
$f5$	Cu(2)-O(2)	35
$f6$	Ba-O(1)	45
$f7$	Ba-O(2)	65
$f8$	Ba-O(3)	35
$f9$	Ba-O(4)	35
$f10$	Y-O(3)	40
$f11$	Y-O(4)	43
$f12$	Cu(2)-Cu(2)	30
$f13$	O(3)-O(3)	10
$f14$	O(4)-O(4)	10
α_1	O(1)-Cu(1)-O(2)	0.2×10^{-18} J rad^{-2}
α_2	O(3)-Cu(2)-O(4)	0.2×10^{-18} J rad^{-2}

The extension to include Coulomb interactions involves the evaluation of an infinite sum of $1/r$ in each element of the dynamical matrix. The necessary transformation which makes the sum rapidly convergent is due to Ewald. Consider a sum of the form

$$F_{\mathbf{k}}(\mathbf{r})=\sum_l\frac{1}{|\mathbf{r}-\boldsymbol{l}|}e^{2\pi i\mathbf{k}\cdot(\boldsymbol{l}-\mathbf{r})}. \quad \text{(A7)}$$

Since it is periodic in $\mathbf{r}$, it can be expressed as a Fourier series,

$$F_{\mathbf{k}}(\mathbf{r})=\sum_{\mathbf{h}}F_{\mathbf{k}}(\mathbf{h})e^{2\pi i\mathbf{h}\cdot\mathbf{r}},$$

$$F_{\mathbf{k}}(\mathbf{h})=\frac{1}{v}\int_{\text{cell}}\sum_l\frac{1}{|\mathbf{r}-\boldsymbol{l}|}e^{2\pi i\cdot[-(\mathbf{h}+\mathbf{k})\cdot\mathbf{r}+\mathbf{k}\cdot\boldsymbol{l}]}d^3r, \quad \text{(A8)}$$

where v is the unit cell volume. By noting that $1/r=2/\sqrt{\pi}\int_0^\infty e^{-r^2\epsilon^2}d\epsilon$, and that $\boldsymbol{l}\cdot\mathbf{h}=$integer, it can be seen that

$$F_{\mathbf{k}}(\mathbf{h})=\frac{2}{v\sqrt{\pi}}\int\int_{\text{cell}}\sum_l e^{-|\mathbf{r}-\boldsymbol{l}|^2\epsilon^2+2\pi i[(\mathbf{k}+\mathbf{h})\cdot(\boldsymbol{l}-\mathbf{r})]}d^3r\,d\epsilon$$

$$=\frac{2}{v\sqrt{\pi}}\int\int e^{-r^2\epsilon^2-2\pi i(\mathbf{k}+\mathbf{h})\cdot\mathbf{r}}d^3r\,d\epsilon$$

$$=\frac{4\sqrt{\pi}}{v}\int\int_0^\infty r^2e^{-r^2\epsilon^2-2\pi i|\mathbf{k}+\mathbf{h}|r\cos\theta}dr\,d\cos\theta\,d\epsilon$$

$$=\frac{2\pi}{v}\int\frac{1}{\epsilon^3}e^{-(\pi^2/\epsilon^2)|\mathbf{k}+\mathbf{h}|^2}d\epsilon. \quad \text{(A9)}$$

Therefore, the original sum could be expressed as

$$F_{\mathbf{k}}(\mathbf{r}) = \frac{2}{\sqrt{\pi}} \sum_{l} \int_{R}^{\infty} e^{-|\mathbf{r}-\boldsymbol{l}|^2\epsilon^2 + 2\pi i \mathbf{k}\cdot(\boldsymbol{l}-\mathbf{r})} d\epsilon + \frac{2\pi}{v} \sum_{\mathbf{h}} \int_{0}^{R} \frac{1}{\epsilon^3} e^{-(\pi^2/\epsilon^2)|\mathbf{k}+\mathbf{h}|^2 + 2\pi i \mathbf{h}\cdot\mathbf{r}} d\epsilon$$
$$= \sum_{l} R \cdot H(|\mathbf{r}-\boldsymbol{l}|R) e^{2\pi i \mathbf{k}\cdot(\boldsymbol{l}-\mathbf{r})} + \frac{1}{\pi v} \sum_{\mathbf{h}} \frac{1}{|\mathbf{k}+\mathbf{h}|^2} e^{-(\pi^2/R^2)|\mathbf{k}+\mathbf{h}|^2 + 2\pi i \mathbf{h}\cdot\mathbf{r}}, \tag{A10}$$

where $H(x) \equiv 2/(\sqrt{\pi}x)\int_x^\infty e^{-y^2} dy$. The series in this form converge very quickly, when a suitable R is chosen. A reasonable choice of R is $(|\mathbf{k}|+1/|\mathbf{r}-\boldsymbol{l}|_{\min})/2$.

Our model follows the one of Chaplot,[28] that is, the two-body interaction is given by

$$\Phi_{dd'}(|\mathbf{r}_d - \mathbf{r}_{ld'}|) = \frac{Z_d Z_{d'}}{|\mathbf{r}_d - \mathbf{r}_{ld'}|} + a e^{-b|\mathbf{r}_d - \mathbf{r}_{ld'}|/(R_d + R_{d'})} \tag{A11}$$

with parameters listed in Ref. 28. After a lengthy but straightforward calculation, the dynamical matrix elements are given by

$$\begin{bmatrix} d & d' \\ \alpha & \alpha' \end{bmatrix} = Z_d Z_{d'} \left\{ \sum_{l} Re^{2\pi i \mathbf{k}\cdot\boldsymbol{l}} H(R|\mathbf{r}-\boldsymbol{l}|)_{\alpha\alpha'}\big|_{\mathbf{r}=\mathbf{r_d}-\mathbf{r_{d'}}} - \frac{4\pi}{v} \sum_{h}{}' \frac{(\mathbf{h}+\mathbf{k})_\alpha (\mathbf{h}+\mathbf{k})_{\alpha'}}{(\mathbf{h}+\mathbf{k})^2} e^{-(\pi^2/R^2)(\mathbf{h}+\mathbf{k})^2 + 2\pi i(\mathbf{h}+\mathbf{k})\cdot(\mathbf{r_d}-\mathbf{r_{d'}})} - \left\langle \frac{4\pi}{v} \frac{\mathbf{k}_\alpha \mathbf{k}_{\alpha'}}{k^2} e^{-(\pi^2/R^2)k^2} \right\rangle \right\}, \quad d \neq d',$$

$$\begin{bmatrix} d & d \\ \alpha & \alpha' \end{bmatrix} = Z_d^2 \left\langle \sum_{l}{}' R(e^{2\pi i \mathbf{k}\cdot\boldsymbol{l}} - 1) H(R|\mathbf{r}-\boldsymbol{l}|)_{\alpha\alpha'}\big|_{\mathbf{r}=\mathbf{0}} - \frac{4\pi}{v} \sum_{h}{}' e^{-(\pi^2/R^2)h^2} \left[\frac{(\mathbf{h}+\mathbf{k})_\alpha (\mathbf{h}+\mathbf{k})_{\alpha'}}{(\mathbf{h}+\mathbf{k})^2} e^{-(\pi^2/R^2)(k^2+2\mathbf{h}\cdot\mathbf{k})} - \frac{\mathbf{h}_\alpha \mathbf{h}_{\alpha'}}{h^2} \right] - \frac{4\pi}{v} \frac{\mathbf{k}_\alpha \mathbf{k}_{\alpha'}}{k^2} e^{-(\pi^2/R^2)k^2} \right\rangle - \sum_{d' \neq d} Z_d Z_{d'} \left\{ \sum_{l} RH(R|\mathbf{r}-\boldsymbol{l}|)_{\alpha\alpha'}\big|_{\mathbf{r}=\mathbf{r_d}-\mathbf{r_{d'}}} - \frac{4\pi}{v} \sum_{h}{}' \frac{\mathbf{h}_\alpha \mathbf{h}_{\alpha'}}{h^2} e^{-(\pi^2/R^2)h^2 + 2\pi i \mathbf{h}\cdot(\mathbf{r_d}-\mathbf{r_{d'}})} \right\}. \tag{A12}$$

The angular brackets above denote that the value enclosed is to taken as zero when $\mathbf{k}=0$. Also, $H(R|\mathbf{r}-\boldsymbol{l}|)_{\alpha\alpha'}$ means $\partial^2 H/\partial r_\alpha \partial r_{\alpha'}$.

APPENDIX B

Throughout this article the dynamical susceptibility (measured for neutron energy loss) is defined as

$$\chi''(\mathbf{q},\omega)_{\text{present}} = \frac{1}{2\pi\hbar} \int dt\ e^{i\omega t} \langle S^-(\mathbf{q},t) S^+(\mathbf{q}) \rangle \tag{B1}$$

or, for an itinerant electron system,

$$\chi''(\mathbf{q},\omega)_{\text{present}} = \sum_{k} (\langle n_{\mathbf{k}\downarrow} \rangle - \langle n_{\mathbf{k}+\mathbf{q}\uparrow} \rangle) \times \delta[E(\mathbf{k}+\mathbf{q}) - E(\mathbf{k}) - \hbar\omega], \tag{B2}$$

where the S's are the dimensionless spin-1/2 operators. We thus quote the dynamical susceptibility per formula unit and in units of inverse energy. This short appendix explicitly compares our definition with other conventions which are also often used.

A convention popular with theorists is

$$\chi''(\mathbf{q},\omega) = \text{Im} \lim_{\epsilon \to 0} \sum_{\mathbf{k}} \frac{\langle n_{\mathbf{k}\downarrow} \rangle - \langle n_{\mathbf{k}+\mathbf{q}\uparrow} \rangle}{E(\mathbf{k}+\mathbf{q}) - E(\mathbf{q}) - \hbar\omega + i\epsilon} \tag{B3}$$

which differs from our convention by a factor of π. Millis and Monien[33] have phrased their discussion in terms of a susceptibility defined by

$$\chi_{xx}(\mathbf{q},\omega) = \int dt\ e^{i\omega t} \langle g\mu_B S_x(\mathbf{q},t) g\mu_B S_x(\mathbf{q}) \rangle = \frac{1}{4} g^2 \mu_B^2 2\pi\hbar \chi''(\mathbf{q},\omega)_{\text{present}}, \tag{B4}$$

where $g=2$ for electrons. As Millis and Monien give their susceptibility per layer instead of per unit cell, their unit convention for $\chi''/\hbar\mu_B^2$ differs by a factor of π from ours.

[1] J. M. Tranquada, G. Shirane, B. Keimer, M. Sato, and S. Shamoto, Phys. Rev. B **40**, 4503 (1989).
[2] S. Shamoto, M. Sato, J. M. Tranquada, B. J. Sternlieb, and G. Shirane, Phys. Rev. B **48**, 13 817 (1993).
[3] J. M. Tranquada, P. M. Gehring, G. Shirane, S. Shamoto, and M. Sato, Phys. Rev. B **46**, 556 (1992), and references therein.
[4] J. Rossat-Mignod, L. P. Regnault, P. Bourges, P. Burlet, C. Vettier, and J. Y. Henry, *Selected Topics in Superconductivity* (World Scientific, Singapore, 1993), and references therein.
[5] J. Rossat-Mignod, L. P. Regnault, C. Vettier, P. Bourges, P. Burlet, J. Bossy, J. Y. Henry, and G. Lapertot, Physica C **185–189**, 86 (1991).
[6] M. Sato, S. Shamoto, T. Kiyokura, K. Kakurai, G. Shirane, B. J. Sternlieb, and J. M. Tranquada, J. Phys. Soc. Jpn. **62**, 263 (1993).
[7] H. A. Mook, M. Yethiraj, G. Aeppli, T. E. Mason, and T. Armstrong, Phys. Rev. Lett. **70**, 3490 (1993).
[8] H. A. Mook, P. Dai, G. Aeppli, T. E. Mason, N. E. Hecker, J. A. Harvey, T. Armstrong, K. Salama, and D. Lee, Physica B **213&214**, 43 (1995).
[9] H. F. Fong, B. Keimer, P. W. Anderson, D. Reznik, F. Dogan, and I. A. Aksay, Phys. Rev. Lett. **75**, 316 (1995).
[10] B. Keimer, H. F. Fong, D. Reznik, F. Dogan, and I. A. Aksay, J. Phys. Chem. Solids **56**, 1927 (1995).
[11] P. Bourges, L. P. Regnault, Y. Sidis, and C. Vettier, Phys. Rev. B **53**, 876 (1996).
[12] D. Z. Liu, Y. Zha, and K. Levin, Phys. Rev. Lett. **75**, 4130 (1995).
[13] I. I. Mazin and V. M. Yakovenko, Phys. Rev. Lett. **75**, 4134 (1995).
[14] F. Onufrieva, Physica C **251**, 348 (1995).
[15] N. Bulut and D. J. Scalapino, Phys. Rev. B **53**, 5149 (1996).
[16] For earlier related theoretical work, see K. Maki and H. Won, Phys. Rev. Lett. **72**, 1758 (1994); P. Monthoux and D. J. Scalapino, *ibid*. **72**, 1874 (1994); H. Fukuyama, H. Kohno, and T. Tanamoto, J. Low Temp. Phys. **95**, 309 (1994); F. Onufrieva and J. Rossat-Mignod, Phys. Rev. B **52**, 7572 (1995).
[17] E. Demler and S. C. Zhang, Phys. Rev. Lett. **75**, 4126 (1995).
[18] V. Barzykin and D. Pines, Phys. Rev. B **52**, 13 585 (1995).
[19] J. S. Lettow, D. L. Milius, E. P. Vicenzo, B. Keimer, and I. A. Aksay (unpublished).
[20] R. J. Cava, B. Batlogg, K. M. Rabe, E. A. Rietman, P. K. Gallagher, and L. W. Rupp, Physica C **156**, 523 (1988).
[21] J. D. Jorgensen, B. W. Veal, A. P. Paulikas, L. J. Nowicki, G. W. Crabtree, H. Claus, and W. K. Kwok, Phys. Rev. B **41**, 1863 (1990).
[22] B. Friedl, C. Thomsen, and M. Cardona, Phys. Rev. Lett. **65**, 915 (1990).
[23] E. Altendorf, X. K. Chen, J. C. Irwin, R. Liang, and W. N. Hardy, Phys. Rev. B **47**, 8140 (1993).
[24] N. Pyka, W. Reichardt, L. Pintschovius, G. Engel, J. Rossat-Mignod, and J. Y. Henry, Phys. Rev. Lett. **70**, 1457 (1993).
[25] D. Reznik, B. Keimer, F. Dogan, and I. A. Aksay, Phys. Rev. Lett. **75**, 2396 (1995).
[26] For a detailed description of the polarized beam technique, see R. M. Moon, T. Riste, and W. C. Koehler, Phys. Rev. **181**, 920 (1969); G. Shirane, *Frontiers of Neutron Scattering* (North-Holland, Amsterdam, 1986).
[27] R. E. Walstedt, B. S. Shastry, and S.-W. Cheong, Phys. Rev. Lett. **72**, 3610 (1994).
[28] S. L. Chaplot, Phys. Rev. B **37**, 7435 (1988).
[29] S. W. Lovesey, *Theory of Neutron Scattering from Condensed Matter* (Clarendon Press, Oxford, 1984).
[30] E. Manousakis, Rev. Mod. Phys. **63**, 1 (1991), and references therein; J. Igarashi, Phys. Rev. B **46**, 10 763 (1992).
[31] These values of the renormalization factors are strictly only valid for the two-dimensional spin-1/2 square-lattice Heisenberg antiferromagnet. To our knowledge, corrections due to interlayer exchange have thus far not been calculated. A recent measurement of Z_χ in $La_{1.86}Sr_{0.14}CuO_4$ (Ref. 34) is consistent with our result.
[32] The small negative values in the subtractions of Fig. 8 around 30 meV are possibly but not necessarily related to normal-state spin excitations. While we have carried out separate measurements of the temperature dependence of the phonon background around 41 meV (Fig. 2), we have not done such measurements around 30 meV.
[33] A. J. Millis and H. Monien (unpublished); Phys. Rev. B **45**, 3059 (1992); *ibid* **50**, 16 606 (1994); A. J. Millis (private communication).
[34] S. M. Hayden, G. Aeppli, H. A. Mook, T. G. Perring, T. E. Mason, S.-W. Cheong, and Z. Fisk, Phys. Rev. Lett. **76**, 1344 (1996).
[35] S. C. Zhang (private communication); K. Levin (private communication); I. I. Mazin (private communication).
[36] J. Ma, C. Quitmann, R. J. Kelley, H. Berger, G. Margaritondo, and M. Onellion, Science **267**, 862 (1995).
[37] F. E. Bates and J. E. Eldridge, Solid State Commun. **64**, 1435 (1987).
[38] W. Kress, U. Schröder, J. Prade, A.D. Kulkarni, and F. W. de Wette, Phys. Rev. B **38**, 2906 (1988).
[39] E. W. Kellermann, Philos. Trans. R. Soc. London **238**, 513 (1940).
[40] J. Humlicek, A. P. Litvinchuk, W. Kress, B. Lederle, C. Thomsen, M. Cardona, H. U. Habermeier, I. E. Trofimov, and W. König, Physica C **206**, 345 (1993).